Dynamically Tunable Singular States Through Air-Slit Control in Asymmetric Resonant Metamaterials

Yeong Hwan Ko * and Robert Magnusson

Posted Date: 9 March 2025

doi: 10.20944/preprints202503.0532.v1

Keywords: lattice resonance; metamaterials and metasurfaces; guided-mode resonance; singular states; equivalent slab waveguide; tunable filters

 doi:10.20944/preprints202503.0532.v1

Article

Dynamically Tunable Singular States Through Air-Slit Control in Asymmetric Resonant Metamaterials

Yeong Hwan Ko [1,*] and Robert Magnusson [2]

[1] Division of Electrical, Electronics, and Control Engineering, Kongju National University, Cheonan 31080, Republic of Korea

[2] Electrical Engineering Department, University of Texas at Arlington, TX 76016 USA; magnusson@uta.edu

* Correspondence: yhk@kongju.ac.kr

Abstract: This study presents a novel method for dynamically tuning singular states in one-dimensional (1D) photonic lattices (PLs) using air-slit-based structural modifications. Singular states are isolated resonance radiations generated by breaking symmetry, which produces various spectra from the interplay between resonance modes and background radiation. By breaking symmetry in 1D PLs with air slits, effective control of resonance positions is demonstrated, enabling dual functionalities including narrowband band pass and notch filtering. These singular states originate from asymmetric guided-mode resonances (aGMRs), which can be interpreted by analytical modeling of equivalent slab waveguide. Furthermore, multiple air-slits significantly enhance spectral tunability by inducing multiple folding behavior in the resonance bands. This approach facilitates effective manipulation of optical properties through simple adjustments of air-slit displacements. This work provides great potential for designing multifunctional photonic devices with advanced metamaterial technologies.

Keywords: lattice resonance; metamaterials and metasurfaces; guided-mode resonance; singular states; equivalent slab waveguide; tunable filters

1. Introduction

Metamaterials and metasurfaces have been widely recognized as transformative platforms for controlling electromagnetic waves [1–3]. These advanced materials utilize subwavelength structures to achieve remarkable electromagnetic properties, such as negative refraction, flat lensing and perfect light absorption and [4–6]. By engineering their composition at the nanoscale, these systems enable accurate control over the amplitude, phase, and polarization of light [7]. Depending on their dimensionality (i.e., 1D, 2D or 3D), these periodic structures provide compact solutions for manipulating light-matter interactions [8–10].

The realization of such advanced materials relies on several physical concepts such as effective medium theory (EMT) [11], lattice resonances [12], particle scattering resonances [13], and surface plasmon effects [14]. EMT uses macroscopic effects from complex subwavelength interactions, which generates extraordinary properties such as negative refractive indices or anisotropic behavior [11,15]. Lattice resonances, namely guided-mode resonances (GMRs), arise from the coupling of guided resonances with diffracted waves in periodic arrays [16,17]. These periodic structures exhibit diverse spectral responses with high quality factor (high-Q) resonances, which enable them highly desirable for wavelength-selective photonic devices [18]. Additionally, particle scattering resonances driven by electric or magnetic dipoles in individual structures facilitate strong light-matter interactions and related phenomena [13,19].

Recently, among various mechanisms, the concept of bound state in the continuum (BIC) has attracted significant attention in metasurface research, which are non-radiative states embedded

 doi:10.20944/preprints202503.0532.v1

within resonance modes under perfect symmetry condition [20,21]. By controlling symmetrical breaking such as off-normal incidence or structural asymmetry, BICs can transition into radiative modes known as quasi-BICs, which shows a great potential for innovative devices including narrowband filtering, optical switching, and biosensing [22–24]. Recent advancements have revealed a new type of resonance in photonic lattices (PLs), where strong resonances radiate immediately at isolated spectral positions from adjacent bands when symmetry is broken. This phenomenon, known as the singular state, represents the realization of quasi-BIC and is explained through asymmetric guided-mode resonances (aGMRs) [25].

In this work, we present a novel method for dynamically tuning singular states by employing PLs with air-slit-based structural modifications. This approach enables effective control over resonance positions and dual functionalities, including narrowband reflection and notch filtering. Furthermore, the introduction of multiple air-slits demonstrates that increasing asymmetry significantly enhances spectral tunability by inducing multiple folding behavior in the resonance bands. These tunable singular states show great potential for designing multifunctional photonic devices.

2. Air Slit Induced Singular States

To investigate tunable singular states, we broke the symmetry of a simple one-dimensional (1D) photonic lattice (PL) by incorporating an air-slit. Figure 1a illustrates the 1D resonant structure, defined by grating parameters such as period (Λ), fill factor (F), and grating height (H) with refractive index (n). Continuing the study of singular states, we employed the previous design of the 1D PL [26] where the grating parameter set is $\{\Lambda = 1\ \mu m,\ F = 0.5,\ H = 0.5\ \mu m\}$ with a lossless material ($n = 2$). In this study, we characterized the zeroth-order reflectance (R_0) using the rigorous coupled-wave analysis (RCWA) [27] method implemented in commercial software [28]. The analysis is performed with TE-polarized light (electric field parallel to the grating grooves) illuminating the 1D PL at normal incidence in the air ($n_{air} = 1$). As shown in calculated R_0 map of Figure 1a, wideband perfect reflection is observed in the spectral region due to the resonant radiation, which has been understood by the guided mode resonance (GMR) phenomenon [16]. As the height (H) increases, additional resonance bands are generated by excitation of higher GMR modes. Figure 1b presents the case where an air-slit with a width of 0.05 μm is introduced at the center of the grating, preserving the structural symmetry. The R_0 map shows resonance bands like those observed without the air-slit (i.e., Figure 1a) but only a slight narrowing observed. This narrowing can be attributed to the effective refractive index reduction due to the presence of air. In contrast, the resonance band is significantly changed when the symmetry is broken by shifting the air-slit. Figure 1c shows the R_0 map of the 1D PL with air slit displaced 0.05 μm from the center. The asymmetry of the 1D PL leads to the formation of a sharp band, which can be interpreted as an off-BIC (bound state in continuum) [20] or asymmetric GMR [25]. Observed in the asymmetric system, these resonance bands can be classified as asymmetric guided-mode resonance (aGMR) modes owing to their origin in asymmetric excitation of GMR modes. Notably, shown in the R_0 map, the fundamental aGMR mode manifests as a singular state, distinctly separated from the other resonance bands. This singular state will be shown to be tunable through manipulation of the air slit.

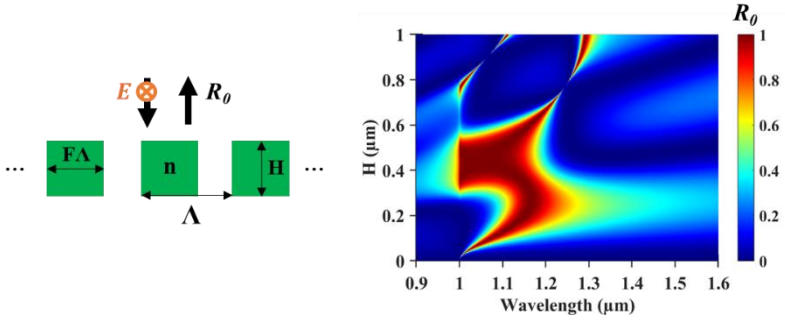

Preprints.org (www.preprints.org) | NOT PEER-REVIEWED | Posted: 9 March 2025 doi:10.20944/preprints202503.0532.v1

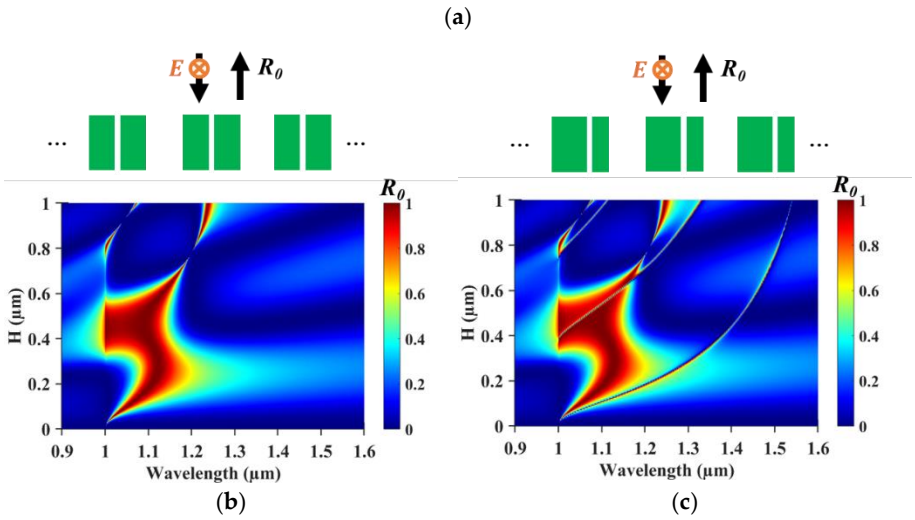

Figure 1. Comparison of symmetric and asymmetric resonant structures. (a) Schematic of the 1D photonic lattice (PL) structure with grating parameters: period (Λ), fill factor (F), and height (H) and refractive index (n). The zeroth-order reflectance (R_0) is calculated for normal incidence with TE-polarized light. (b) Schematic and R_0 map for the symmetric air-slit 1D PL as a function of wavelength and the H. (c) Schematic and R_0 map for the asymmetric air-slit 1D PL under the same conditions, showing sharp resonances due to broken symmetry.

3. Interpretation of Singular States

Singular states can be interpreted by analyzing the slab waveguide modes of an equivalent 1D PL. As depicted in Figure 2a, the 1D PL can be approximated as a slab waveguide where electromagnetic fields are confined through the coupling of diffracted waves to a propagation constant (β). For this equivalent slab waveguide, the 1D grating layer is homogenized using effective medium theory (EMT) with the Rytov's formalism [29]. The effective refractive indices (n_m^{TE} and v_m^{TE}) are determined by the mth order solutions from the following equations [29,30]:

$$\frac{\sqrt{n^2-(n_m^{TE})^2}}{\sqrt{1-(n_m^{TE})^2}} = \frac{tan\left\{\frac{\pi\Lambda}{\lambda}(1-F)\sqrt{1-(n_m^{TE})^2}\right\}}{tan\left\{\frac{\pi\Lambda}{\lambda}F\sqrt{n^2-(n_m^{TE})^2}\right\}} \quad \text{(symmetric)}, \quad (1)$$

$$\frac{\sqrt{n^2-(v_m^{TE})^2}}{\sqrt{1-(v_m^{TE})^2}} = \frac{tan\left\{\frac{\pi\Lambda}{\lambda}F\sqrt{n^2-(n_m^{TE})^2}\right\}}{tan\left[\frac{\pi\Lambda}{\lambda}(1-F)\sqrt{1-(v_m^{TE})^2}\right]} \quad \text{(asymmetric)}. \quad (2)$$

Here, the n_m^{TE} and v_m^{TE} represent the symmetric and asymmetric field EMT solutions from each equation (1) and (2). Considering the first diffraction waves, we apply the first solution n_1^{TE} and v_1^{TE} for slab waveguide analysis. The eigenvalue problem of the lth TE mode of slab waveguide can be expressed as [25,31]:

$$tan\left\{q_1\frac{H}{2}-l\frac{\pi}{2}\right\} = \frac{\sqrt{(\beta)^2-(k_0)^2}}{q_1} \qquad l=0,1,\ldots, \quad (3)$$

where the q_1 and k_0 are vertical propagation vectors of first-order diffracted waves and propagation constant ($2\pi/\lambda$) in vacuum, respectively. Based on the different EMT solutions (n_1^{TE} and v_1^{TE}), the q_1 is given by $n_1^{TE}k_0$ or $v_1^{TE}k_0$. The β represents the propagation constant of the guided mode, assuming coupled from the first-order grating vector ($K=2\pi/\Lambda$). Consequently, the lth TE guided modes (TE_l or aTE_l) are obtained as eigen-solutions using symmetric and asymmetric effective refractive indices. Figure 2b displays the calculated TE_l or aTE_l modes, which matches the resonance bands observed in the asymmetric air slit 1D PL in Figure 1c. Indeed, the singular state originates from the aTE_0, indicating the fundamental guided mode of asymmetric EMT slab coupled by first-order diffracted waves.

Preprints.org (www.preprints.org) | NOT PEER-REVIEWED | Posted: 9 March 2025 doi:10.20944/preprints202503.0532.v1

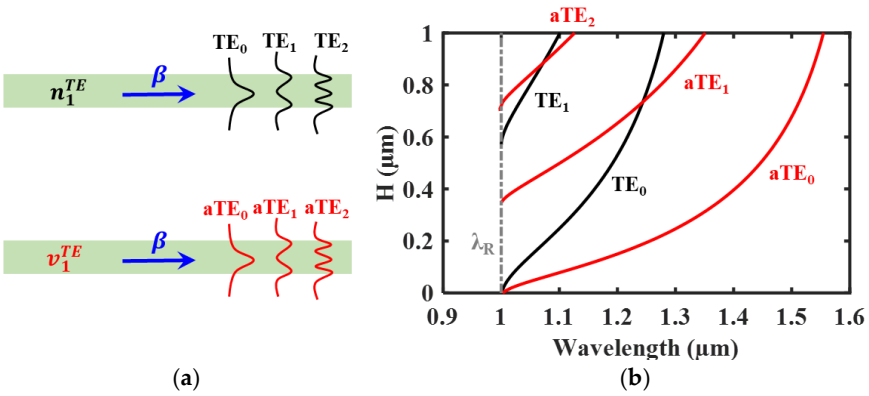

Figure 2. Analytical modeling for the resonant 1D PLs. (a) Schematic of equivalent slab waveguides, where the 1D PL is homogenized using effective medium theory (EMT). The diffracted light is coupled to symmetric (TE_0, TE_1, TE_2) and asymmetric (aTE_0, aTE_1, aTE_2) guided modes, determined by effective refractive indices (n_1^{TE} for symmetric modes and v_1^{TE} for asymmetric modes) and propagation constant (β). (b) Calculated guided modes as a function of slab height (H). Symmetric modes are represented in black, and asymmetric modes are shown in red. The vertical dashed line indicates Rayleigh wavelength (λ_R=$n_{air}\Lambda$).

4. Analysis of Air Slit-Induced Singular States

To characterize the aTE_0 mode of the singular state, we analyze the electric field profiles at specific points on the R_0 spectra of both the symmetric and asymmetric air-slit 1D PLs, as depicted in Figure 2b and Figure 2c. Figure 3a shows these points (i)-(iv) on the R_0 spectra for the air slit 1D PLs. In contrast to point (i) on the spectrum of the symmetric air-slit 1D PL (black dash line), the point (ii) on the asymmetric air-slit 1D PL (red solid line) spectrum exhibits a sharp resonance peak at λ=1.4266 μm, associated with a singular state. In shorter wavelength region, the point (iii) corresponds high reflection while point (iv) shows a sharp dip at λ=1.0734 μm. The electric field distributions (E_y, as out of plane) corresponding to these points are presented in Figure 3b to 3e. As shown in Figure 3b, the light propagates through the 1D PL without resonance. In Figure 3c, however, the light is strongly confined to the lattice with asymmetric air-slit. This E_y profile represents the singular state, formed by the fundamental guided modes (i.e., aTE_0). In Figure 3d, the light is highly reflected from the symmetric air-slit 1D PL. Conversely, in Figure 3e, it passes through in the asymmetric air-slit 1D PL due to interaction with enhanced E_y field, forming the first guided modes (i.e., aTE_1).

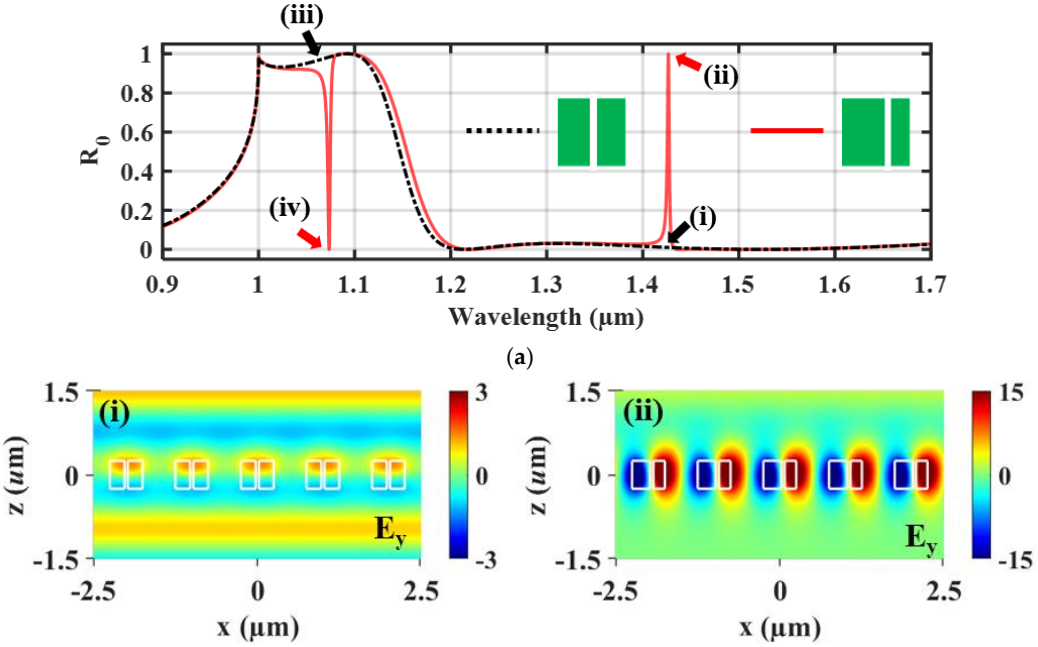

 doi:10.20944/preprints202503.0532.v1

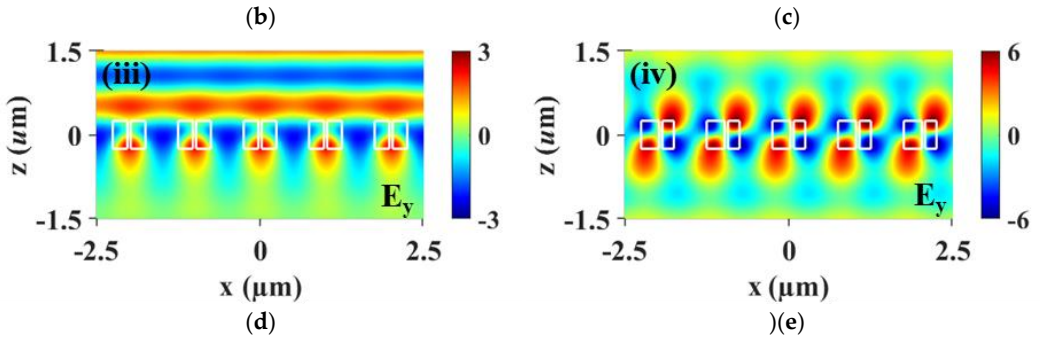

Figure 3. Electromagnetic field analysis for air slit-induced singular states. (a) The R_0 spectra for symmetric (black dashed line) and asymmetric (red solid line) air-slit 1D PLs. Points (i)-(iv) indicate specific spectral positions for symmetric and asymmetric air-slit 1D PLs. (b)-(e) Electric field (E_y, as out of plane) distributions at points (i)-(iv), respectively.

5. Tunable Singular States by Asymmetric Air-Slit 1D Lattice

Prior to designing tunable singular states, we examine the refractive index (n) effects on the singular state in the asymmetric air-slit 1D PL. Figure 4a presents the R_0 map for the symmetric air-slit 1D PL where the spectral response is calculated by varying the n from 1.5 to 3.5. As observed, two resonance bands shift toward longer wavelengths as n increases. This red shift is a characteristic behavior of GMRs as higher n increases a propagation constant of guided mode. Figure 4b shows the corresponding R_0 map for the asymmetric air-slit case under the same refractive index variations. As expected, sharp resonance bands appear and exhibit a red shift. Notably, the singular state becomes increasingly isolated from the other resonance bands for higher refractive index material as silicon nitride (Si_3N_4, n ≈ 2) and silicon (Si, n ≈ 3.5).

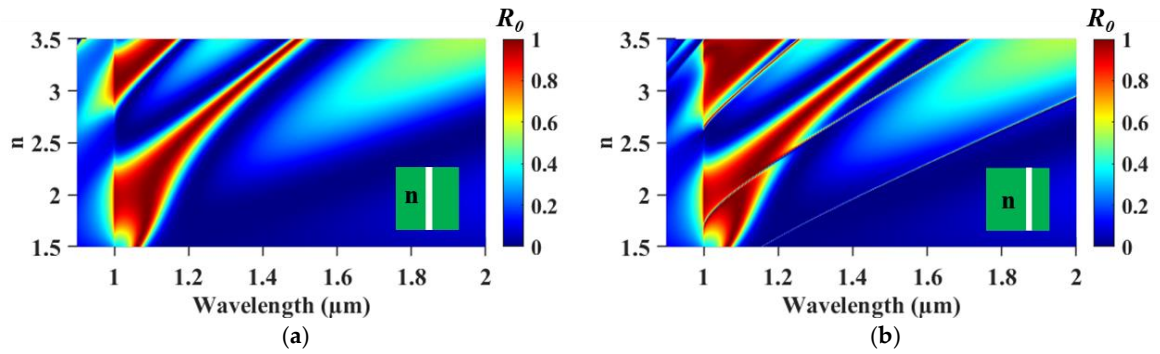

Figure 4. Refractive index effects on the singular state. (a) R_0 map for the symmetric air-slit 1D PL as a function refractive index (n). (b) Corresponding (a) Reflectance (R_0) map for the symmetric air-slit 1D PL as a function of the n. The first sharp resonance band becomes increasingly isolated as the n increases.

The aGMR enables the generation of tunable singular state by varying asymmetry of the air-slit 1D PL. Figure 5 shows the tunable singular state in an air-slit 1D PL based on a dielectric material (n=2), where the grating parameter set is {Λ = 1 μm, F = 0.5, H = 0.5 μm}. As illustrated in the schematic of Figure 5, a single air-slit with a width of 0.05 μm is displaced by a distance d from the symmetric line. In the R_0 map of the asymmetric air-slit 1D PL, two sharp resonances are observed due to the aGMRs. The lower peak corresponds to the aTE_0 mode, while the upper dip represents the aTE_1 mode. These modes arise from the interference between leaky waveguide modes and background radiation, as a phenomenon characteristic of Fano resonances [32]. At the low reflection region, the R_0 peak can be used as a notch filter. In contrast, the R_0 dip around the high reflection band for band pass filter. When the d gradually increases from zero to $\pm$0.15 μm, these dual functionalities can be simultaneously tuned by varying the d.

Preprints.org (www.preprints.org) | NOT PEER-REVIEWED | Posted: 9 March 2025 doi:10.20944/preprints202503.0532.v1

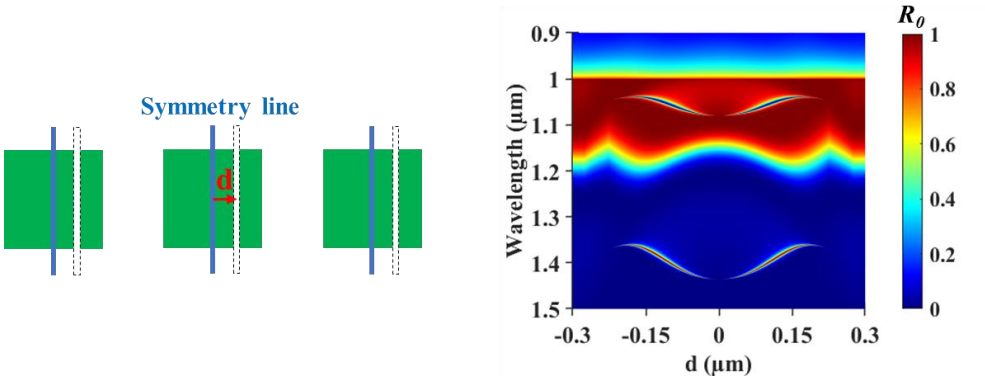

Figure 5. Tunable singular state by variation of a single air-slit. Modeling for asymmetric single slit 1D PL. The grating parameters are the same as for Figure 3a. A single air-slit with a width of 0.05 μm is displaced by a distance d from the symmetric line. The R_0 map shows two sharp resonances corresponding to the aTE_0 and aTE_1 modes.

This dual functionality becomes even more dynamic with the introduction of multiple air-slits. As shown in the schematic of Figure 6a, two air-slits are aligned with a pitch width of $F\Lambda/2$=0.25 μm. By varying the displacement d from zero to ±0.35 μm, as seen in R_0 map of Figure 6b, the two sharp aGMRs are rapidly tuned. This behavior corresponds to the one-fold radiation observed in the single air-slit case of Figure 5. Using triple and quadruple air-slits, the aGMRs exhibit even faster tuning due to two- and three-fold radiation effects as presented in Figures 6c and Figure 6d. Herein, the triple and quadruple air-slits are equally distributed within the same pitch width ($F\Lambda/2$=0.25 μm). These additional slits introduce more degrees of asymmetry, thus leading to more change of the spectral position of the aGMRs. Meanwhile, these resonances shift toward shorter wavelengths (blue-shift) as the number of air-slits increases because the effective refractive index is reduced by more air gaps. This ability to dynamically tune singular states by simply adjusting the multiple air-slit promise for applications in metamaterials and metasurfaces.

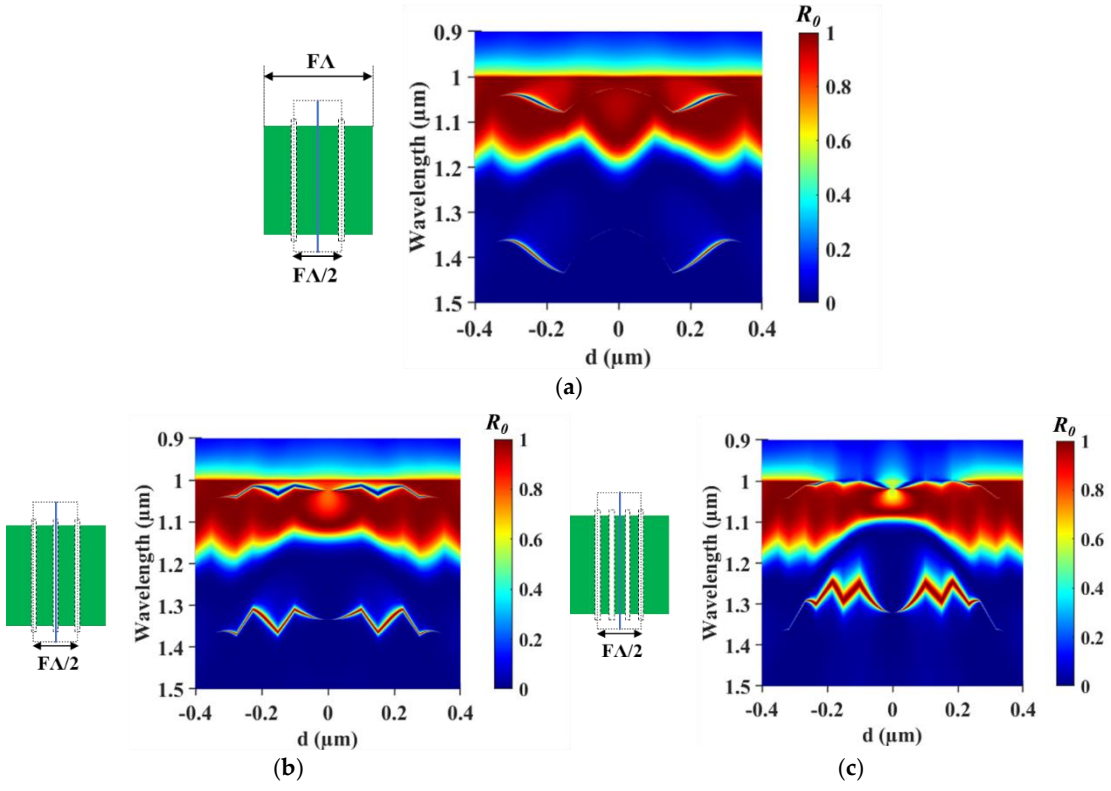

 doi:10.20944/preprints202503.0532.v1

Figure 6. Tunable singular states in multi-slit asymmetric 1D PLs. (a) Schematic of the double air-slit, where two air-slits are separated by a pitch of $F\Lambda/2$, and the displacement d is varied from the symmetric center line. The corresponding R_0 map shows dynamically shifting resonance as the d increases. Schematics and R_0 maps are also compared for (b) triple and (c) quadruple air-silts. Each slit is evenly distributed with the same pitch ($F\Lambda/2$). As the number of air-slits increases, the resonance positions shift more dynamically, exhibiting multiple folding behavior of the resonances.

6. Conclusions

In conclusion, the asymmetric guided-mode resonance (aGMR) mechanism enables the radiation of tunable singular states by varying the structural asymmetry of photonic lattices (PLs) through air-slits. Our analysis demonstrates that the air-slit induced singular state can effectively control the spectra position of strong resonance interfering with background radiation. Through systematic investigation, we have shown that the refractive index plays a critical role in determining the spectral position and isolation of singular states. Dielectric materials such as silicon nitride (Si_3N_4) and silicon (Si) are proper for realizing tunable singular states due to their high refractive indices and compatible fabrication technologies. Furthermore, the multiple air-slits significantly enhance the tunability of singular states, which enables dynamic control over resonance positions through multiple folding behavior of resonances. By displacing the air-slits, dual functionalities (i.e., narrowband band pass filter and notch filtering) are achieved. It expects to be useful for versatile metasurface and metamaterial applications in optical filters, switches and photonic devices. Despite potential fabrication challenges such as precise air-slit alignment and symmetry control, these structures are feasible with advanced nanofabrication techniques. The proposed concepts are extendable to other spectral regions and polarization-independent designs by 2D metastructures. This work will be useful for developing highly tunable optical devices for photonic applications.

Author Contributions: Conceptualization, Y.K.; methodology, Y.K.; formal analysis, Y.K; investigation, Y.K.; writing—original draft preparation, Y.K.; R.M.; project administration, R.M.; funding acquisition, R.M. All authors have read and agreed to the published version of the manuscript.

Funding: This research was supported, in part, by the UT System Texas Nanoelectronics Research Superiority Award funded by the State of Texas Emerging Technology Fund and by the Texas Instruments Distinguished University Chair in Nanoelectronics endowment.

Institutional Review Board Statement: Not applicable.

Informed Consent Statement: Not applicable.

Data Availability Statement: The data underlying the results presented in this paper are not publicly available at this time but may be obtained from the authors upon reasonable request.

Conflicts of Interest: The authors declare no conflicts of interest. The authors declare that they have no known competing financial interest or personal relationships that could have appeared to influence the work reported in this paper.

References

1. Ji, W.; Chang, J.; Xu, H.-X.; Gao, J.R.; Gröblacher, S.; Urbach, H.P.; Adam, A.J.L. Recent advances in metasurface design and quantum optics applications with machine learning, physics-informed neural networks, and topology optimization methods. *Light Sci. Appl*. **2023**, 12, 169.
2. Armelles, G.; Bergamini, L.; Zabala, N.; García, F.; Dotor, M.L.; Torné, L.; Alvaro, R.; Griol, A.; Martínez, A.; Aizpurua, J.; et al. Metamaterial Platforms for Spintronic Modulation of Mid-Infrared Response under Very Weak Magnetic Field. *ACS Photonics* **2018**, 5, 3956-3961.
3. Su, V.-C.; Chu, C.H.; Sun, G.; Tsai, D.P. Advances in optical metasurfaces: fabrication and applications [Invited]. *Opt. Express* **2018**, 26, 13148-13182.
4. Jakšić, Z.; Vuković, S.; Matovic, J.; Tanasković, D. Negative Refractive Index Metasurfaces for Enhanced Biosensing. *Materials* **2011**, 4, 1-36.

 doi:10.20944/preprints202503.0532.v1

5. Banerji, S.; Meem, M.; Majumder, A.; Vasquez, F.G.; Sensale-Rodriguez, B.; Menon, R. Imaging with flat optics: metalenses or diffractive lenses? *Optica* **2019**, 6, 805-810.
6. Roger, T.; Vezzoli, S.; Bolduc, E.; Valente, J.; Heitz, J.J.F.; Jeffers, J.; Soci, C.; Leach, J.; Couteau, C.; Zheludev, N.I.; et al. Coherent perfect absorption in deeply subwavelength films in the single-photon regime. *Nat. Commun*. **2015**, 6, 7031.
7. Overvig, A.C.; Shrestha, S.; Malek, S.C.; Lu, M.; Stein, A.; Zheng, C.; Yu, N. Dielectric metasurfaces for complete and independent control of the optical amplitude and phase. *Light Sci. Appl*. **2019**, 8, 92.
8. Chen, J.; Xiao, J.; Lisevych, D.; Shakouri, A.; Fan, Z. Deep-subwavelength control of acoustic waves in an ultra-compact metasurface lens. *Nat. Commun*. **2018**, 9, 4920.
9. Luo, X. Subwavelength Optical Engineering with Metasurface Waves. *Adv. Opt. Mater*. **2018**, 6, 1701201.
10. Hu, Y.; Luo, X.; Chen, Y.; Liu, Q.; Li, X.; Wang, Y.; Liu, N.; Duan, H. 3D-Integrated metasurfaces for full-colour holography. *Light Sci. Appl*. **2019**, 8, 86.
11. Zhang, X.; Wu, Y. Effective medium theory for anisotropic metamaterials. *Sci. Rep*. **2015**, 5, 7892.
12. Ko, Y.H.; Razmjooei, N.; Hemmati, H.; Magnusson, R. Perfectly-reflecting guided-mode-resonant photonic lattices possessing Mie modal memory. *Opt. Express* **2021**, 29, 26971-26982.
13. Van de Groep, J.; Polman, A. Designing Dielectric Resonators on Substrates: Combining Magnetic and Electric Resonances. *Opt. Express* **2013**, 21, 26285-26302.
14. Genevet, P.; Capasso, F.; Aieta, F.; Khorasaninejad, M.; Devlin, R. Recent Advances in Planar Optics: From Plasmonic to Dielectric Metasurfaces. *Optica* **2017**, 4, 139-152.
15. Chen, X.; Grzegorczyk, T.M.; Wu, B.-I.; Pacheco, J.; Kong, J.A. Robust method to retrieve the constitutive effective parameters of metamaterials. *Phys. Rev. E* **2004**, 70, 016608.
16. Wang, S.S.; Magnusson, R. Theory and applications of guided-mode resonance filters. *Appl. Opt*. **1993**, 32, 2606-2613.
17. Huang, L.; Jin, R.; Zhou, C.; Jiang, Y.; Jia, Y.; Gao, Y.; Xu, L.; Hu, W.; Gao, J.; Song, Q. Ultrahigh-Q guided mode resonances in an All-dielectric metasurface. *Nat. Commun*. **2023**, 14, 3433.
18. Magnusson, R.; Wang, S.S. New principle for optical filters. *Appl. Phys. Lett*. **1992**, 61, 1022-1024.
19. Murai, S.; Castellanos, G.W.; Raziman, T.V.; Curto, A.G.; Rivas, J.G. Enhanced Light Emission by Magnetic and Electric Resonances in Dielectric Metasurfaces. *Adv. Opt. Mater*. **2020**, 8, 1902024.
20. Marinica, D.C.; Borisov, A.G.; Shabanov, S.V. Bound States in the Continuum in Photonics. *Phys. Rev. Lett*. **2008**, 100, 183902.
21. Azzam, S.I.; Kildishev, A.V. Photonic Bound States in the Continuum: From Basics to Applications. *Adv. Opt. Mater*. **2021**, 9, 2001469.
22. Liu, Y.; Zhang, Q.; Xing, X.; Zou, D.; Mao, B.; Yao, J.; Ouyang, C.; Wang, Z.; Wu, L. Terahertz narrowband filter metasurfaces based on bound states in the continuum. *Opt. Express* **2023**, 31, 35272-35281.
23. Che, Y.; Zhang, T.; Shi, T.; Deng, Z.-L.; Cao, Y.; Guan, B.-O.; Li, X. Ultrasensitive Photothermal Switching with Resonant Silicon Metasurfaces at Visible Bands. *Nano Lett*. **2024**, 24, 576-583.
24. Liu, B.; Peng, Y.; Jin, Z.; Wu, X.; Gu, H.; Wei, D.; Zhu, Y.; Zhuang, S. Terahertz ultrasensitive biosensor based on wide-area and intense light-matter interaction supported by QBIC. *Chem. Eng. J*. **2023**, 462, 142347.
25. Ko, Y.H.; Hemmati, H.; Magnusson, R. Quantifying bound and leaky states of resonant optical lattices by Rytov-equivalent homogeneous waveguides. *Opt. Lett*. **2023**, 48, 311-314.
26. Ko, Y.H.; Lee, K.J.; Simlan, F.A.; Magnusson, R. Singular states of resonant nanophotonic lattices. *Nanophotonics* **2023**, 12, 263-272.
27. Moharam, M.G.; Grann, E.B.; Pommet, D.A.; Gaylord, T.K. Formulation for Stable and Efficient Implementation of the Rigorous Coupled-Wave Analysis of Binary Gratings. *J. Opt. Soc. Am. A* **1995**, 12, 1068-1076.
28. RSoft Products. DiffractMod; Synopsys, Inc.: Sunnyvale, CA, USA, **2025**.
29. Rytov, S.M. Electromagnetic properties of a finely stratified medium. *Sov. Phys. JETP* **1956**, 2, 466-475.
30. Hemmati, H.; Magnusson, R. Applicability of Rytov's Full Effective-Medium Formalism to the Physical Description and Design of Resonant Metasurfaces. *ACS Photonics* **2020**, 7, 3177-3187.

 doi:10.20944/preprints202503.0532.v1

31. Adams, M.J. An Introduction to Optical Waveguides; Wiley: Chichester, UK, **1981**.
32. Yoon, J.W.; Magnusson, R. Fano resonance formula for lossy two-port systems. *Opt. Express* **2013**, 21, 17751-17759.